

Narrow graphene nanoribbons from carbon nanotubes

Liyang Jiao^{1*}, Li Zhang^{1*}, Xinran Wang¹, Georgi Diankov¹ & Hongjie Dai¹

Graphene nanoribbons (GNRs) are materials with properties distinct from those of other carbon allotropes^{1–5}. The all-semiconducting nature of sub-10-nm GNRs could bypass the problem of the extreme chirality dependence of the metal or semiconductor nature of carbon nanotubes (CNTs) in future electronics^{1,2}. Currently, making GNRs using lithographic^{3,4,6}, chemical^{7–9} or sonochemical¹ methods is challenging. It is difficult to obtain GNRs with smooth edges and controllable widths at high yields. Here we show an approach to making GNRs by unzipping multi-walled carbon nanotubes by plasma etching of nanotubes partly embedded in a polymer film. The GNRs have smooth edges and a narrow width distribution (10–20 nm). Raman spectroscopy and electrical transport measurements reveal the high quality of the GNRs. Unzipping CNTs with well-defined structures in an array will allow the production of GNRs with controlled widths, edge structures, placement and alignment in a scalable fashion for device integration.

The high carrier mobility of graphene^{10–14} offers the possibility of building high-performance graphene-based electronics. Recently, both theoretical^{15–18} and experimental^{1–4} works have shown that quantum confinement and edge effects introduce a band gap in narrow graphene ribbons independent of chirality, and the resulting GNR semiconductors can be used to make field-effect transistors. Several approaches have been developed to obtain GNRs. Lithographic patterning has been used to produce wide ribbons (>20 nm) from graphene sheets^{3,4}, but the width and smoothness of the GNRs were limited by the resolution of the lithography and etching techniques. Bulk amounts of wide (20–300 nm) and few-layered (2–40) GNRs were synthesized by a chemical vapour deposition method⁹. A chemical sonication route developed by our group produced sub-10-nm GNR semiconductors from intercalated and exfoliated graphite¹. However, the yield of GNRs was low and their width distribution was broad; widths ranged from less than 10 nm to ~100 nm.

Because CNTs are considered to be GNRs rolled up into seamless tubes and the synthesis, size control, placement and alignment control of nanotubes have been widely investigated and established^{19,20}, we ask the question of whether CNTs can be unzipped to form GNRs with structural control. The greatest challenge in converting CNTs to GNRs is to develop ways of cleaving CNTs in the longitudinal direction without rapid etching along the circumference.

Here we develop controlled unzipping of CNTs to produce GNRs by an Ar plasma etching method. To remove a longitudinal strip of carbon atoms from the side walls of CNTs, we first embedded multi-walled carbon nanotubes (MWCNTs) in a poly(methyl methacrylate) (PMMA) layer as an etching mask (Fig. 1). Briefly, pristine MWCNTs (diameter, ~4–18 nm; see Supplementary Fig. 1a) synthesized by arc discharge (Bucky tube, Aldrich) were dispersed in 1% surfactant solution by brief sonication and deposited onto a Si

substrate. A 300-nm-thick film of PMMA was spin-coated on top of the MWCNTs. After baking, the PMMA–MWCNT film was peeled off in a KOH solution²¹ (Fig. 1b). MWCNTs embedded in the resulting PMMA film had a narrow strip of side wall not covered by PMMA, owing to conformal PMMA coating on the substrate. The PMMA–MWCNT film was then exposed to a 10-W Ar plasma for various times (Fig. 1c). Owing to protection by the PMMA, the top side walls of MWCNTs were etched faster and removed by the plasma. Single-, bi- and multilayer GNRs and GNRs with inner CNT cores (Fig. 1d–g) were produced depending on the diameter and number of layers of the starting MWCNT and the etching time. After etching, the PMMA film was contact-printed and attached to a Si substrate with a 500-nm-thick layer of SiO₂. Finally, the PMMA film was removed using acetone vapour²¹, and this was followed by calcination at 300 °C for 10 min to remove polymer residue on the target substrate, leaving GNRs on the substrate (Fig. 1h).

The mean diameter of our starting MWCNTs was ~8 nm (Fig. 2a and Supplementary Fig. 1a). For 10 s of Ar plasma etching, our method converted ~20% of the MWCNTs into single- or few-layer GNRs of 10–20-nm width (height, <2 nm; see Fig. 2). Other products were multilayer GNRs or GNRs with CNT cores (Fig. 1d). The yield of GNRs was limited by the relatively wide diameter distribution of the starting MWCNTs used (Supplementary Information). All of the width data were obtained after correcting the tip-size effect¹. Within

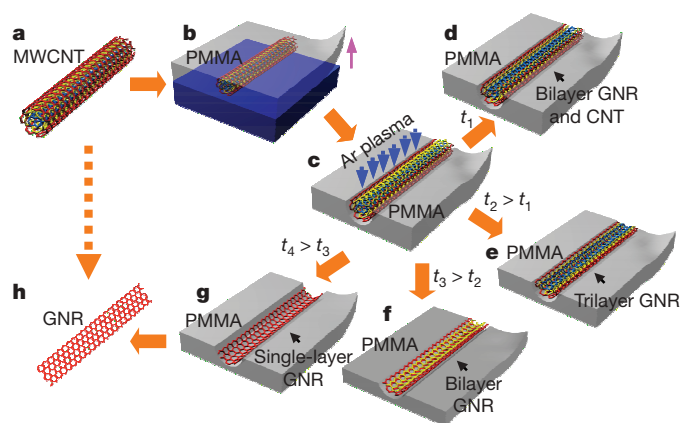


Figure 1 | Making GNRs from CNTs. **a**, A pristine MWCNT was used as the starting raw material. **b**, The MWCNT was deposited on a Si substrate and then coated with a PMMA film. **c**, The PMMA–MWCNT film was peeled from the Si substrate, turned over and then exposed to an Ar plasma. **d–g**, Several possible products were generated after etching for different times: GNRs with CNT cores were obtained after etching for a short time t_1 (**d**); tri-, bi- and single-layer GNRs were produced after etching for times t_2 , t_3 and t_4 , respectively ($t_4 > t_3 > t_2 > t_1$; **e–g**). **h**, The PMMA was removed to release the GNR.

¹Department of Chemistry and Laboratory for Advanced Materials, Stanford University, Stanford, California 94305, USA.

*These authors contributed equally to this work.

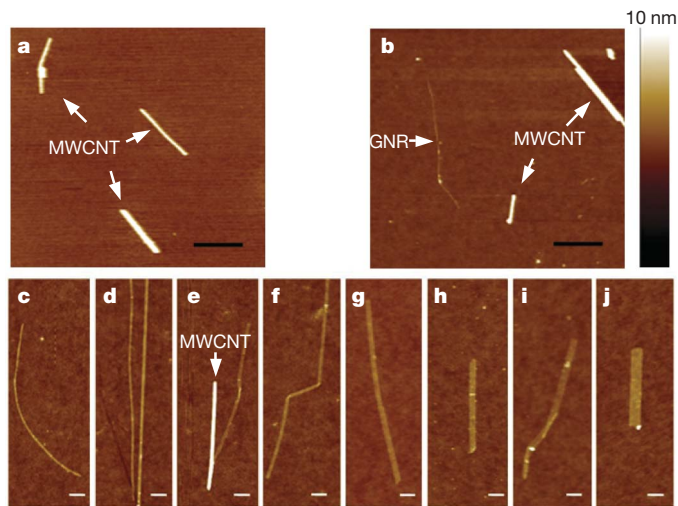


Figure 2 | Images of GNRs converted from MWCNTs. **a**, An AFM image of raw MWCNTs dispersed on a Si substrate. **b**, An image of the substrate after the GNR conversion process, showing coexistence of MWCNTs and GNRs. Scale bars, 1 μm . **c–j**, Single- or few-layer GNRs of different widths and heights: respectively 7 and 1.8 nm (**c**), 8 and 1.8 nm (left, **d**), 13 and 2.0 nm (right, **d**), 15 and 0.9 nm (**e**), 17 and 1.0 nm (**f**), 25 and 1.1 nm (**g**), 33 and 1.4 nm (**h**), 45 and 0.8 nm (**i**) and 51 and 1.9 nm (**j**). Scale bars, 100 nm. The height scale for all the AFM images is 10 nm. In **e**, an arrow points to a leftover MWCNT.

the resolution of atomic force microscopy (AFM), the edges of the obtained GNRs were very smooth. Unlike for previous GNRs, the ribbons were uniform in width along their lengths, none being wedge shaped¹, owing to the quasi-one-dimensional CNT templates with uniform diameter along their lengths. According to histogram data on GNRs (Supplementary Fig. 1b, c), the widths of our GNRs mostly fell into the range 10–20 nm, which is narrower than that of GNRs made by the sonochemical method¹. The width of 10–20 nm corresponds to half of the circumference of the starting MWCNTs with the

mean diameter of ~ 8 nm. The heights of our GNRs were ~ 0.8 , 1.3 and 1.8 nm, which we assign to single-, bi- and trilayer GNRs, respectively²². The folding observed in single-layer GNRs (Fig. 2e, f, i) suggests that the flexibility of the GNRs is excellent in comparison with that of MWCNTs. The folds resulted from bending of the PMMA film²³ and/or the perturbation of liquid during the removal of the PMMA in acetone.

Raman spectroscopy is a powerful approach to investigating the structural and electronic properties of carbon-based materials. The shape of the second-order Raman band (2D) is a characteristic that can be used to distinguish the number of layers of AB-stacked graphene^{24–26}. We carried out confocal Raman mapping on single-, bi- and trilayer GNRs (Methods). We obtained an AFM image (Fig. 3a) and a G-band image (Fig. 3b) of a 0.9-nm-thick GNR on the same length scale. The 2D peak was well fitted by a sharp and symmetric Lorentzian peak (inset, Fig. 3c), suggesting the single-layer nature of the GNR. For another 1.3-nm-thick GNR (Fig. 3d–f), the 2D peak was fitted by four Lorentzians (inset, Fig. 3f), characteristic of bilayer, AB-stacked graphene. Some bilayer GNRs showed 2D peaks with different line shapes from AB-stacked graphene, reflecting the varying stacking structures between layers in the starting MWCNTs (Supplementary Fig. 2). For a trilayer GNR (height, ~ 1.9 nm; see Supplementary Fig. 3), similar to trilayer, ABA-stacked graphene sheets, the 2D band was broader and up shifted as the thickness increased (Supplementary Table 1). We note that the 2D band of the MWCNTs was broader than that of our GNRs (Supplementary Fig. 6), as expected.

The intensity ratio of the D and G bands (I_D/I_G) is commonly used to evaluate the quality of carbon materials. No obvious D band was observed for any of the MWCNTs dispersed on substrates (Supplementary Fig. 6), suggesting the high quality of the starting materials. The average I_D/I_G values were respectively 0.38, 0.30 and 0.28 for our single-, bi- and trilayer GNRs with 10–20-nm widths. Because defect density on the pristine MWCNTs was low, the D-band Raman signal of our GNRs should be mainly due to their open edges^{24,25}. The I_D/I_G values were lower than those for GNRs obtained

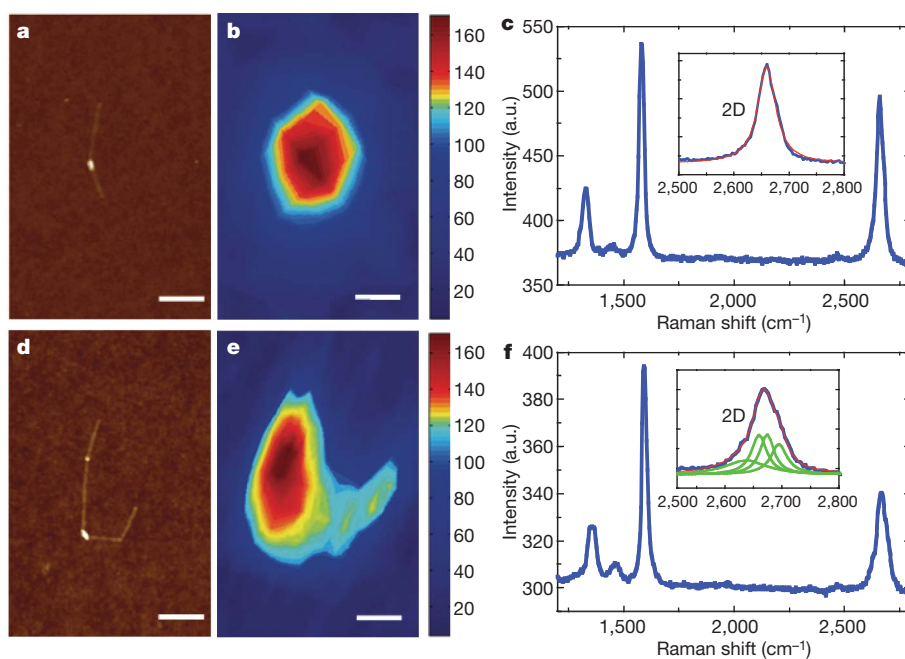


Figure 3 | Raman imaging and spectra of GNRs. **a–c**, An AFM image (**a**), a G-band Raman image (**b**) and the Raman spectrum (**c**) of a single-layer GNR. Inset of **c**, a 2D-band spectrum (blue) of the GNR and a single-Lorentzian fit (red). a.u., arbitrary units. **d–f**, An AFM image (**d**), a G-band Raman image (**e**) and the Raman spectrum (**f**) of a bilayer GNR. Inset of **f**, 2D band

spectrum (blue) of the GNR and the best-fit curve (red), which is a combination of four Lorentzians (green). The $\sim 1,440$ cm^{-1} peaks in **c** and **f** are attributed to trace PMMA left on the SiO_2 (Supplementary Fig. 4). Scale bars, 200 nm.

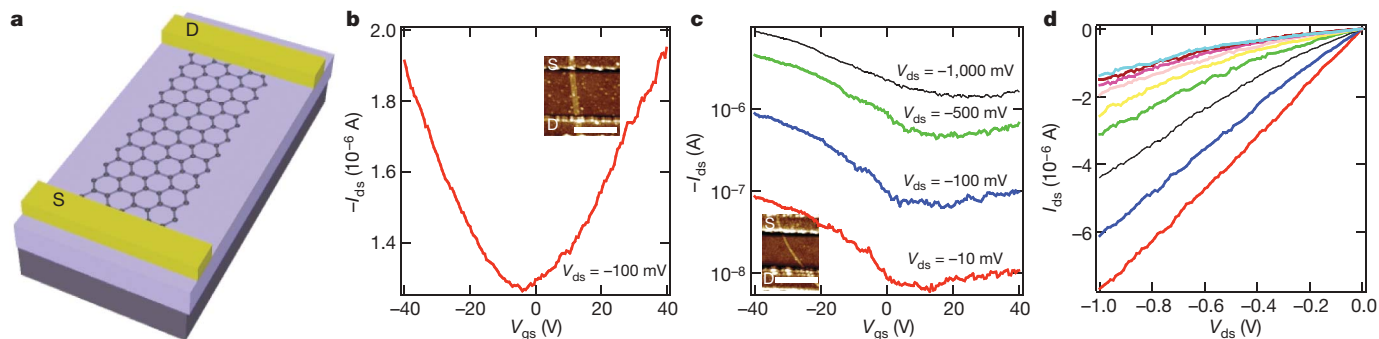


Figure 4 | Room-temperature electrical properties of GNR devices. **a**, A GNR device. S, source; D, drain. **b**, Plot of drain–source current (I_{ds}) versus gate–source voltage (V_{gs}) for a ~ 16 -nm-wide GNR device probed in vacuum after electrical annealing. The Dirac point is near $V_g = 0$ V. Inset, AFM image of this device; scale bar, 200 nm. **c**, I_{ds} – V_{gs} curves for a ~ 7 -nm-wide GNR

device at various biases probed in air (inset, AFM image; scale bar, 200 nm). The ratio of on-state current (I_{on}) to off-state current (I_{off}) for this GNR device is ~ 10 . **d**, I_{ds} – V_{ds} curves for the device in **c** at gate biases V_{gs} ranging from -40 V (bottom) to 40 V (top) in steps of 10 V.

by lithographic etching of pristine graphene sheets (I_D/I_G was ~ 2 for a bilayer GNR of ~ 28 -nm width obtained by lithographic patterning (X. R. Wang *et al.*, unpublished data); see Supplementary Fig. 5), indicating the high quality of our GNRs, in particular the high degree of edge smoothness.

There are several key steps in making GNRs from MWCNTs using our approach. Embedding MWCNTs in a PMMA film as an etching mask is essential to protect parts of the shells of the MWCNTs from plasma. The relatively low viscosity and good wetting capability of PMMA allowed its conformal coating on the MWCNTs. The choice of plasma source is also critical to longitudinally unzip CNTs. O_2 plasma was widely used for chemical etching of carbon materials. However, control experiments found that O_2 plasma etching tended to remove complete shells from MWCNTs, even with the partial protection of PMMA (Supplementary Fig. 7), suggesting that the chemical etching of MWCNTs by O_2 plasma was rapid along the nanotube circumference and could not be used to produce GNRs. The bombardment effect of Ar plasma²⁷ offered anisotropic physical etching to remove atoms at unprotected sites along the longitudinal direction of the CNTs. To make the etching more controllable, we used a low plasma power of 10 W and optimized the etching time. We found that longer etching duration increased the yield of single- and few-layer GNRs, but caused breaks in the GNRs. After etched for 20 s and longer, ribbons tended to be discontinuous and have frequent cuts. Raman spectra of GNRs obtained by etching for 30 s showed high I_D/I_G values, of > 1.0 (Supplementary Fig. 8). Inhomogeneity in MWCNT diameter and number of layers caused variation in the GNR number of layers and the residue CNT structures. By using a starting CNT material with a controlled shell number and diameter, we expect to obtain GNRs of a well-defined width and number of layers at $\sim 100\%$ yield.

We fabricated three-terminal devices with our GNRs (Fig. 4), with Pd as source and drain contacts (channel length, $L \approx 250$ nm), a p++ Si back gate and thermally grown 500 -nm SiO_2 as gate dielectrics. GNRs ≤ 10 nm in width showed field-effect transistor characteristics with p-doping effects due to the physisorbed O_2 from ambient and other species during the treatment steps (Fig. 4c and Supplementary Fig. 9). A ~ 7 -nm-wide GNR device had an I_{on}/I_{off} ratio of > 10 (Fig. 4c) and a ~ 6 -nm-wide GNR device had $I_{on}/I_{off} > 100$ (Supplementary Fig. 9). These GNRs had quantum-confined semiconducting characteristics, rather than those of bulk graphene, with much weaker gate modulation of conductance. We note that the error bar in widths measured by AFM was ± 2 – 3 nm, which led to relatively large uncertainties in the measured widths in the sub- 10 -nm region. To obtain GNR devices with higher I_{on}/I_{off} values, even narrower GNRs are needed and could be obtained by our method by using few-walled CNTs.

Our > 10 -nm-wide GNR devices showed weaker gate dependence (Fig. 4b) owing to smaller band gaps, consistent with lithographically

and chemically derived GNRs of similar widths^{1,3,4}. Figure 4b shows the transfer characteristics of a ~ 16 -nm-wide GNR device probed in vacuum after electrical annealing²⁸ by applying a bias of up to 3 V. The GNR exhibited a clear conductance minimum corresponding to the Dirac point at $V_g \approx 0$ V after electrical annealing by removing physisorbed O_2 and other p-doping species (Supplementary Fig. 10). The ‘V’-shaped I_{ds} – V_{gs} curve of the GNR device resembles that of bulk graphene, reflecting symmetric hole and electron transports at negative and positive gate voltages, respectively. The resistivity of the devices at the Dirac point for our 10 – 20 -nm-wide GNRs was 10 – 40 k Ω , similar to lithographically patterned 20 – 50 -nm-wide GNRs^{3,22,29}. The fact that the resistivity of our GNRs is comparable to that of the lithographically patterned ones suggests a similar quality of GNRs in the 10 – 20 -nm width range. The mobilities of the GNRs made by both methods were also similar and ~ 10 times lower than those of large two-dimensional graphene sheets, most likely because of edge scattering in the GNRs^{10–12}.

Unzipping of CNTs offers a new way of producing GNRs with controlled structure and quality. Our approach is also compatible with semiconductor processing. Progress made in the synthesis, size control, placement and alignment control of CNTs can be exploited to make GNRs in a controlled fashion. CNTs with narrower diameter and chirality distributions can be used to make GNRs with well-defined widths and edge structures. Few-walled CNTs can be used to obtain narrow, sub- 10 -nm, GNRs with band gaps sufficient for room-temperature transistor applications. Aligned CNT arrays can lead to GNR arrays. Thus, it should be possible to produce large-scale, well-aligned semiconducting GNRs with controlled structures for practical application in electronics.

METHODS SUMMARY

Preparation of GNRs. We dispersed 1 mg of MWCNTs in 10 ml of 1% Tween 20 aqueous solution by sonication for 5 min and then centrifugation at $16,400g$ for 10 min to remove aggregates. The MWCNT suspension was deposited onto a Si substrate pretreated with 3-aminopropyltriethoxysilane (APTES, 12 ml in 20 ml of H_2O), rinsed with water and then blow-dried. The sample was then calcined at $350^\circ C$ for 10 min to remove the Tween 20. A PMMA solution (relative molecular mass, $M_w = 495,000$; 5% in anisole) was spin-coated on MWCNTs on the substrate at $3,000$ rounds per minute for 1 min and then baked at $170^\circ C$ for 2 h on a hot plate. The PMMA–MWCNT film was peeled off in 1 M KOH solution at $80^\circ C$ (ref. 21). Then the film was rinsed with water and printed onto a Si substrate. To make the film well-adhered to the Si substrate, we heated the sample at $80^\circ C$ for 10 min in an oven. Ten-watt Ar plasma was used to etch the PMMA–MWCNT film at the base pressure of 40 mTorr. After etching, we lifted the PMMA film using water and then adhered it to an APTES-treated, 500 -nm SiO_2/Si substrate with a prefabricated Pt/W marker array. After the PMMA had been removed using acetone vapour²¹, the obtained sample was calcined at $300^\circ C$ for 10 min to remove the residue of PMMA.

Fabrication of GNR devices. We located the GNRs with AFM and recorded their locations relative to the prefabricated Pt/W markers. The source–drain electrode

pattern was then designed to provide electrical contact to the GNRs; this was carried out by electron beam lithography, 20-nm Pd metal deposition and lift off. The devices were then annealed in Ar at 220 °C for 15 min to improve the contact quality. Electrical characterization of the devices was carried out both in air and in vacuum using a semiconductor analyser (Agilent 4156C).

Characterization of GNRs using Raman spectroscopy. Raman spectra of individual GNRs located by AFM were measured using a 633-nm HeNe laser (spot size, $\sim 1 \mu\text{m}$) and a power of $\sim 1 \text{ mW}$. The mapping area was set to be $3 \mu\text{m} \times 3 \mu\text{m}$ and the step size was 100 nm. The D, G and 2D bands were recorded and the integration time was 10 s at each spot.

Received 30 December 2008; accepted 16 February 2009.

- Li, X. L. *et al.* Chemically derived, ultrasmooth graphene nanoribbon semiconductors. *Science* **319**, 1229–1232 (2008).
- Wang, X. R. *et al.* Room-temperature all-semiconducting sub-10-nm graphene nanoribbon field-effect transistors. *Phys. Rev. Lett.* **100**, 206803 (2008).
- Chen, Z. H., Lin, Y. M., Rooks, M. J. & Avouris, P. Graphene nano-ribbon electronics. *Physica E (Amsterdam)* **40**, 228–232 (2007).
- Han, M. Y., Ozyilmaz, B., Zhang, Y. B. & Kim, P. Energy band-gap engineering of graphene nanoribbons. *Phys. Rev. Lett.* **98**, 206805 (2007).
- Cresti, A. *et al.* Charge transport in disordered graphene-based low dimensional materials. *Nano Res.* **1**, 361–394 (2008).
- Tapasztó, L., Dobrik, G., Lambin, P. & Biro, L. P. Tailoring the atomic structure of graphene nanoribbons by scanning tunnelling microscope lithography. *Nature Nanotechnol.* **3**, 397–401 (2008).
- Datta, S. S., Strachan, D. R., Khamis, S. M. & Johnson, A. T. C. Crystallographic etching of few-layer graphene. *Nano Lett.* **8**, 1912–1915 (2008).
- Ci, L. J. *et al.* Controlled nanocutting of graphene. *Nano Res.* **1**, 116–122 (2008).
- Campos-Delgado, J. *et al.* Bulk production of a new form of sp^2 carbon: crystalline graphene nanoribbons. *Nano Lett.* **8**, 2773–2778 (2008).
- Novoselov, K. S. *et al.* Electric field effect in atomically thin carbon films. *Science* **306**, 666–669 (2004).
- Zhang, Y. B., Tan, Y. W., Stormer, H. L. & Kim, P. Experimental observation of the quantum Hall effect and Berry's phase in graphene. *Nature* **438**, 201–204 (2005).
- Novoselov, K. S. *et al.* Two-dimensional gas of massless Dirac fermions in graphene. *Nature* **438**, 197–200 (2005).
- Berger, C. *et al.* Electronic confinement and coherence in patterned epitaxial graphene. *Science* **312**, 1191–1196 (2006).
- Geim, A. K. & Novoselov, K. S. The rise of graphene. *Nature Mater.* **6**, 183–191 (2007).
- Nakada, K., Fujita, M., Dresselhaus, G. & Dresselhaus, M. S. Edge state in graphene ribbons: nanometer size effect and edge shape dependence. *Phys. Rev. B* **54**, 17954–17961 (1996).
- Barone, V., Hod, O. & Scuseria, G. E. Electronic structure and stability of semiconducting graphene nanoribbons. *Nano Lett.* **6**, 2748–2754 (2006).
- Son, Y. W., Cohen, M. L. & Louie, S. G. Energy gaps in graphene nanoribbons. *Phys. Rev. Lett.* **97**, 216803 (2006).
- Yang, L. *et al.* Quasiparticle energies and band gaps in graphene nanoribbons. *Phys. Rev. Lett.* **99**, 186801 (2007).
- Dai, H. J. Carbon nanotubes: opportunities and challenges. *Surf. Sci.* **500**, 218–241 (2002).
- Jorio, A., Dresselhaus, M. S. & Dresselhaus, G. *Carbon Nanotubes: Advanced Topics in the Synthesis, Structure, Properties and Applications.* (Springer, 2008).
- Jiao, L. Y. *et al.* Creation of nanostructures with poly(methyl methacrylate)-mediated nanotransfer printing. *J. Am. Chem. Soc.* **130**, 12612–12613 (2008).
- Lin, Y. M. & Avouris, P. Strong suppression of electrical noise in bilayer graphene nanodevices. *Nano Lett.* **8**, 2119–2125 (2008).
- Jiao, L. Y., Xian, X. J. & Liu, Z. F. Manipulation of ultralong single-walled carbon nanotubes at macroscale. *J. Phys. Chem. C* **112**, 9963–9965 (2008).
- Ferrari, A. C. *et al.* Raman spectrum of graphene and graphene layers. *Phys. Rev. Lett.* **97**, 187401 (2006).
- Graf, D. *et al.* Spatially resolved Raman spectroscopy of single- and few-layer graphene. *Nano Lett.* **7**, 238–242 (2007).
- Ni, Z. H., Wang, Y. Y., Yu, T. & Shen, Z. X. Raman spectroscopy and imaging of graphene. *Nano Res.* **1**, 273–291 (2008).
- Winters, H. F., Coburn, J. W. & Chuang, T. J. Surface processes in plasma-assisted etching environments. *J. Vac. Sci. Technol. B* **1**, 469–480 (1983).
- Moser, J., Barreiro, A. & Bachtold, A. Current-induced cleaning of graphene. *Appl. Phys. Lett.* **91**, 163513 (2007).
- Lin, Y. M., Perebeinos, V., Chen, Z. H. & Avouris, P. Electrical observation of subband formation in graphene nanoribbons. *Phys. Rev. B* **78**, 161409 (2008).

Supplementary Information is linked to the online version of the paper at www.nature.com/nature.

Acknowledgements This work was supported by Microelectronics Advanced Research Corporation - Materials, Structures, and Devices Center, Intel and the US Office of Naval Research.

Author Information Reprints and permissions information is available at www.nature.com/reprints. Correspondence and requests for materials should be addressed to H.D. (hdai@stanford.edu).